IEEE Access
Multidisciplinary | Rapid Review | Open Access Journal

Received December 2, 2019, accepted December 17, 2019, date of publication December 23, 2019, date of current version January 9, 2020.

Digital Object Identifier 10.1109/ACCESS.2019.2961810

A Stacked Autoencoder Neural Network Algorithm for Breast Cancer Diagnosis With Magnetic Detection Electrical Impedance Tomography

RUIJUAN CHEN[1], WEIWEI WU[1], HAOFENG QI[1], JINHAI WANG[1,2], AND HUIQUAN WANG[1,2]

[1]School of Life Sciences, Tiangong University, Tianjin 300387, China
[2]Tianjin Key Laboratory of Optoelectronic Detection Technology and Systems, Tianjin 300387, China

Corresponding author: Huiquan Wang (huiquan85@126.com)

This work was supported in part by the National Natural Science Foundation of China under Grant 81901789.

ABSTRACT Magnetic detection electrical impedance tomography (MDEIT) is a novel imaging technique that aims to reconstruct the conductivity distribution with electrical current injection and the external magnetic flux density measurement by magnetic sensors. Aiming at improving the resolution and accuracy of MDEIT and providing an efficient imaging method for breast cancer diagnosis, a new algorithm based on stacked auto-encoder (SAE) neural network is proposed. Both numerical simulation and phantom experiments are done to verify its feasibility. In the numerical simulation, an amount of sample data with different conductivity distribution are calculated. Then a neural network model is established and trained by training these samples. Finally, the conductivity distribution of an imaging target with the anomaly location can be reconstructed by the network model. The reconstruction result of the SAE algorithm is compared with the reconstruction results of the traditional sensitivity matrix (SM) algorithm and the back propagation (BP) neural network algorithm. Under the noise of 30dB, the relative errors of BP algorithm, SM algorithm and SAE algorithm are 137.19%, 24.90% and 15.28% respectively. Result shows by the SAE algorithm, the location of anomalies is reconstructed more accurately, the conductivity value is more closely to the real one and the anti-noise performance is more robust. At last, a breast phantom experiment by self-made platforms is completed to verify the application feasibility of the new algorithm. The relative reconstruction error of conductivity by proposed SAE algorithm can be reduced to 14.56%. The results show that by SAE algorithm, MDEIT can be a promising approach in clinical diagnosis of breast cancer, and it also provide more potential application prospect for the extensive application of MDEIT.

INDEX TERMS Breast cancer diagnosis, inverse problem, magnetic detection electrical impedance tomography, stacked auto-encoder.

I. INTRODUCTION

Breast cancer is one of the most common cancers among women in the world [1]. High precision of medical imaging modalities is required to discriminate tumors in early time diagnosis for breast cancer. It will avert the unnecessary biopsy, ameliorate the cancer treatment strategy and boost the patient's survival rate. Currently breast cancer testing has been studied in a variety of imaging modalities. Traditional imaging methods for breast cancer involve mammography [2], B-ultrasonic imaging [3], magnetic resonance imaging [4], and so on. None of them is ideal because of radiation, low resolution or high cost. Magnetic detection electrical impedance tomography (MDEIT) is a novel imaging modality to reconstruct the conductivity distribution by measuring the magnetic flux density surrounding the imaging object [5], [6]. Considering that the measurement of magnetic flux density does not require surface contact, the sensor fixing problems of tradition Electrical impedance tomography (EIT) [7] is eliminated in MDEIT and a great number of

The associate editor coordinating the review of this manuscript and approving it for publication was Qi Zhou.

measurements can be recorded with precise detector positions [8]. Therefore, compared to the traditional EIT, MDEIT has the advantages of non-contact sensing, less electrodes, and extensive application domains [9], [10]. In the medical engineering, we can use MDEIT to monitor the physiological state and pathological information of the human body by reconstructing the electrical property information using pairs of excitation electrodes and a number of magnetic induction coils placed around the imaging target [11]. In the energy and electricity field, the topology and breakpoints of the grounding grid can be detected by MDEIT [12]. However, although the reconstruction can be improved a lot compared with traditional EIT, there is still problems pending further development in MDEIT such as the spatial and temporal image resolution [13].

The inverse problem of MDEIT is ill-posed. Sensitivity matrix algorithm (SM algorithm) [14] with regularization techniques has been used to solve the conductivity reconstruction in MDEIT such as total variation (TV) methods [15], [16], joint L-1 and TV regularization methods [17] et al. Although regularized reconstruction methods have been shown to be effective in dealing with simple imaging tasks, their limited capability may cause difficulties in coping with more complicated imaging targets. Recently, deep learning is widely used in many fields such as fault detection [18]–[20], image processing [21], emotion recognition [22], and so on. Some scholars also tried to applied deep learning models to the reconstruction of inverse problems [23], [24]. Convolutional neural network (CNN) is proposed to solve inverse problem of the electrical resistance tomography (ERT), the accuracy of reconstructed image is improved and the reconstruction time is shortened [25]. Artificial neural network (ANN) is proposed to improve the resolution of reconstructed images [26]. The conductivity value of the three-dimensional human brain is accurately reconstructed by radial basis neural network (RBFNN) [27]. According to the previous research, a multi-input multi-output MDEIT imaging algorithm based on stacked auto-encoder (SAE) neural network is proposed to solve the reconstruction of the inverse problem. The main purpose of the proposed SAE neural network algorithm is to significantly improve the quality of the image and the speed of reconstruction. Both numerical simulation and phantom experiment results show the effectiveness of the algorithm. The advantages of the algorithm in reconstruction accuracy, anti-noise performance and reconstruction speed are verified by comparing the reconstruction image with the reconstruction results of back propagation (BP) neural network algorithm and sensitivity matrix (SM) algorithm. With the SAE neural network algorithm, the value of conductivity can be accurately reconstructed and the position of the anomaly can be determined. The SAE algorithm effectively improves the ill-posed of MDEIT inverse problem. It provides a new and promising approach for MDEIT image reconstruction. It also provides a fast and high-precision imaging method for the diagnosis of breast tumors.

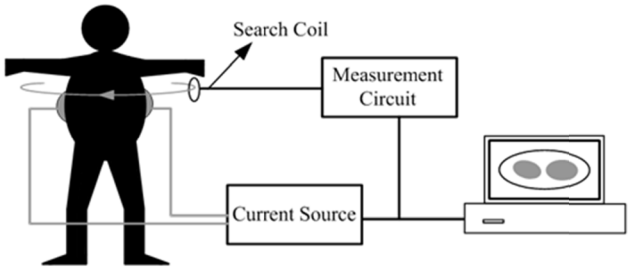

FIGURE 1. Principle of magnetic detection electrical impedance tomography.

II. BASIC AND KEY TECHNOLOGIES

There are two main aspects in MDEIT: forward problem and inverse problem. The forward problem computes the distributions of voltage, current density within an electrically conducting domain and magnetic flux density surrounding the object from the known conductivity distribution according to the boundary value problem and Biot-Savart law. The inverse problem uses the measured magnetic flux density data to reconstruct the conductivity distribution.

A. FORWARD PROBLEM IN MDEIT

Under the stimulation of the excitation current with low-

frequency, the capacitive characteristic of biological tissue can be neglected, and only the conductivity characteristic can be considered so that the imaging object can be approximated as an ionic conductor in this case [28]. Fig. 1 shows the principle of MDEIT. With an excitation current injected into the imaging body, the external magnetic induction intensity can be measured by coils.

Assume the conductivity of the imaging object is $\boldsymbol{\sigma}$, with a current injection $\boldsymbol{I_0}$, the voltage $\boldsymbol{\varphi}$, and current density distribution $\boldsymbol{J}$ are produced in the imaging body. From Maxwell equations and Ohm's law, we can formulate the Laplace equation, as show in (1).

$$\boldsymbol{\nabla \cdot \sigma \nabla \varphi = 0} \tag{1}$$

It meets the Newman boundary conditions, as shown in (2).

$$-\boldsymbol{\sigma \frac{\partial \varphi}{\partial n} = J_n} \tag{2}$$

where n is the normal unit vector at the boundary, and $\boldsymbol{J_n}$ is the current density at the boundary with the current injection. The electrical potential can be obtained by solving the equation above with the Finite Element Method (FEM). Then the current density can be obtained by:

$$\boldsymbol{J = -\sigma \nabla \varphi} \tag{3}$$

Finally, according to Biot-Savart's law, the magnetic induction intensity of the imaging area can be obtained by:

$$\boldsymbol{B_{(r)} = \frac{\mu_0}{4\pi} \int_{\Omega} J_{(r)} \times \frac{r - r'}{|r - r'|^3} d\Omega} \tag{4}$$

where $\boldsymbol{u_0}$ is the permeability of vacuum and also nonmagnetic objects, $\boldsymbol{B_{(r)}}$ is the external magnetic flux density of the

imaging object, $\boldsymbol{r} = (\boldsymbol{x}, \boldsymbol{y})$ is the position vector of the measurement point, and $\boldsymbol{r}' = \left(\boldsymbol{x}', \boldsymbol{y}'\right)$ is the position vector of the source of current density.

In summary, since the external magnetic flux density of the imaging object reflects the conductivity distribution inside the imaging body, we can obtain the conductivity distribution of an object by inverse algorithms.

B. SENSITIVITY MATRIX ALGORITHM FOR INVERSR PROBLEM

SM algorithm is mainly based on linearization of the variation of a magnetic flux density due to conductivity perturbations. It initially assumes a uniform conductivity distribution and calculates a current density distribution with the finite element method (FEM) the same with the forward problem of conventional EIT. Next, the magnetic flux density $\boldsymbol{B_0}$ can be described according to the Biot-Savart law. Then, suppose there is a conductivity perturbation $\boldsymbol{\Delta\sigma}$ in the imaging region around the uniform values, then the current density change correspondingly causes an increment of magnetic flux density as $\boldsymbol{\Delta B}$ [29]. According to the SM algorithm, define the sensitivity matrix as $\mathbf{S}$, then the total matrix equation can be represented as:

$$\boldsymbol{\Delta B} = \boldsymbol{S\Delta\sigma} \tag{5}$$

Once the sensitivity matrix S is obtained, the conductivity perturbation $\boldsymbol{\Delta\sigma}$ causing variation of the magnetic flux density $\boldsymbol{\Delta B}$ can be solved by (5). Then, the course can be iterated by replacing $\boldsymbol{\sigma_0}$ with $\boldsymbol{\sigma_0} + \boldsymbol{\Delta\sigma}$ until the termination condition is satisfied [30]. In this paper, the termination condition is defined as whether the norm of $\boldsymbol{\Delta B}$ is larger than the previous iteration.

C. BP NEURAL NETWORK ALGORITHM FOR INVERSE PROBLEM

In order to reconstruct the conductivity distribution through the magnetic field measurement data, this paper uses the BP algorithm based on Scaled Conjugate Gradient (SCG) [31] to train the BP network parameters and apply it to solve the MDEIT inverse problem.

The neural network has three layers of neurons, the first layer is the input layer, through which the neurons input the magnetic induction value B to the neural network; the second layer is the hidden layer; the third layer is the output layer, which outputs the conductivity inside the imaged body. The process of training the neural network includes: propagating the training data forwardly to establish a neural network and then backpropagation update the weight matrix. The conductivity was reconstructed using a trained neural network. Fig. 2 is a basic structure diagram of the BP neural network.

D. SAE ALGORITHM FOR INVERSE PROBLEM

In order to realize the reconstruction of conductivity distribution by the magnetic field measurement data, this paper proposes a SAE neural network algorithm connected with

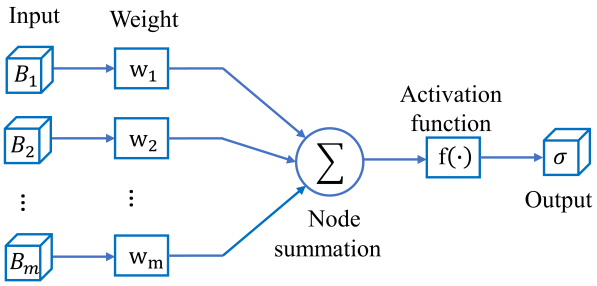

FIGURE 2. Basic structure diagram of BP Neural Network.

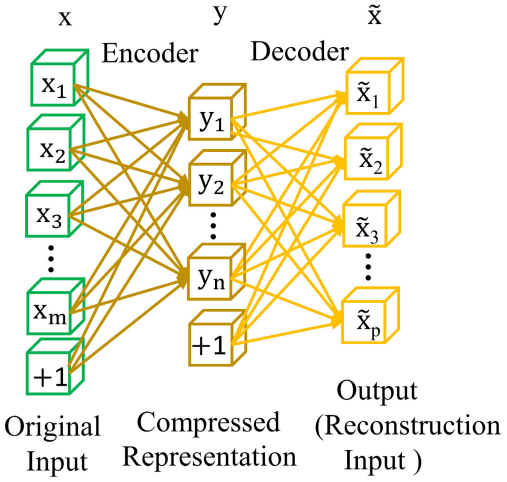

FIGURE 3. A basic schema of an auto-encoder.

softmax classifier to solve the inverse problem of MDEIT. The stacked auto-encoder neural network, referred to as SAE in this paper, is a feedback neural network model consisting of a series of multi-layer auto-encoders (AE) [32]. AE is an unsupervised feature learning method, and the softmax classifier is a supervised learning algorithm, the SAE model combines the advantages of unsupervised and supervised together [33], [34].

A typical AE is a neural network consisting of three fully connected layers: the input layer, the hidden layer, and the output layer. The neurons between layers are entirely inter connected, as shown in Fig. 3. Given a set of training sample $\boldsymbol{B} = \{\boldsymbol{b_1}, \boldsymbol{b_2}, \boldsymbol{b_3}, \ldots, \boldsymbol{b_m}\}$ (m is the number of training samples) as the input parameter $\boldsymbol{x}$, where the $\boldsymbol{i^{th}}$ input layer neuron can be represented by $\boldsymbol{b_i}$. The number of neurons in the hidden layer is $\boldsymbol{n}$, the $\boldsymbol{j^{th}}$ hidden layer neuron can be represented by $\boldsymbol{y_j}$.The weight matrix between the input layer and the hidden layer in this paper is as (6):

$$\begin{pmatrix} \boldsymbol{w_{11}} & \cdots & \boldsymbol{w_{1j}} \\ \vdots & \ddots & \vdots \\ \boldsymbol{w_{i1}} & \cdots & \boldsymbol{w_{ij}} \end{pmatrix} \tag{6}$$

where $\boldsymbol{w_{ij}}$(i $= 1, 2, 3 \ldots$ m; j $= 1, 2, 3 \ldots$ n) represents the weight of the $\boldsymbol{i^{th}}$ input layer neuron to the $\boldsymbol{j^{th}}$ hidden layer neuron. The auto-encoder uses the first layer of the neural

network to convert the input vector into a hidden vector using an activation function. In this study we used the logistic sigmoid function as (7):

$$f(t) = \frac{1}{1+e^{-t}} \tag{7}$$

The process from the input layer to the output of hidden layer neurons, called encoding, is obtained by:

$$y = f(t) = f\left(\sum_{i=1}^{m} w_{ij}x_i + b_j\right) \tag{8}$$

where b_j is the bias of the j^{th} hidden layer neuron. The process of converting the hidden layer data into the output layer data is called decoding, and the output data can be obtained as (9):

$$\tilde{x}_i = f\left(\sum_{j=1}^{n} w_{ij}^T y_j + b_i^{'}\right) \tag{9}$$

where $b_i^{'}$ is the bias of the i^{th} input layer neuron. The parameters of this neural network are optimized to minimize the average reconstruction error $J(w, b)$:

$$J(w, b) = \frac{1}{M}\sum_{k=1}^{M} L\left(x^{(k)}, \tilde{x}^{(k)}\right) \tag{10}$$

where L is a loss function. The Gradient Descent method is used to update the weight matrices and the bias vectors according to (11)-(13).

$$w = w - \alpha\frac{\partial L(x,\tilde{x})}{\partial w} \tag{11}$$

$$b = b - \alpha\frac{\partial L(x,\tilde{x})}{\partial b} \tag{12}$$

$$b^{'} = b^{'} - \alpha\frac{\partial L(x,\tilde{x})}{\partial b^{'}} \tag{13}$$

where α represents the learning rate.

The deep neural network model based on SAE used in this study is constructed by two auto-encoder layers, with the output of the encoder in the previous layer as the input to the encoder of the subsequent layer [35]. The weight matrices of the neural network include a feature extraction matrix, feature coding matrix, and classification reconstruction matrix [36], [37]. Each hidden layer of the neural network is the higher abstraction of the previous layer, so the last hidden layer, softmax classifier, contains the high-level structure and representative information of the imaging object's conductivity distribution. The basic structure of SAE is shown in Fig. 4.

The feature extraction matrix extracts the feature of input magnetic flux density distribution, and highlights the feature information. Feature information is encoded by the feature coding matrix. The classification reconstruction matrix located between the second hidden layer and the output layer classified the coding features to obtain an n-type label, and the conductivity distribution information is carried in this n-type label.

In this algorithm, we put magnetic flux density to the input data and get the conductivity as the output. SAE classifier can extract and analyze the characteristics between the magnetic flux density and the conductivity distribution. With the optimization process mentioned above, the conductivity parameter can be reconstructed.

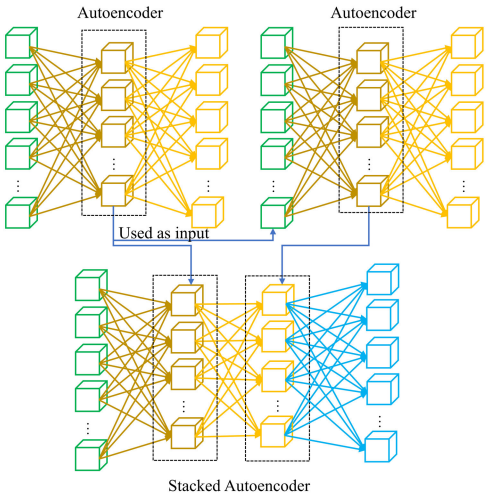

FIGURE 4. The structure of the SAE.

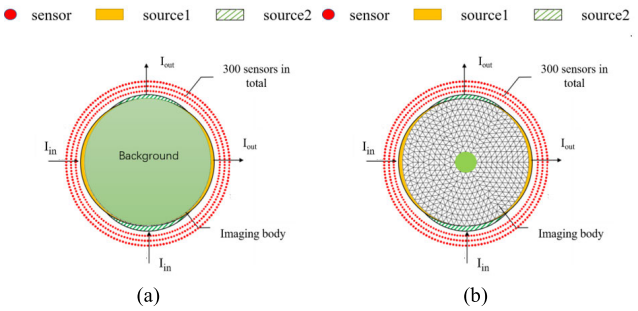

FIGURE 5. A uniform simulation model (a) and a simulation model (b) with an anomaly.

III. EXPERIMENT

A. SIMULATION EXPERIMENT

In order to test the SAE algorithm, numerical simulation experiment is completed. We compare the numerical solution using the new algorithm with the SM algorithm and BP algorithm. A circular imaging body is used to simulate the two-dimensional section of human breast. Fig. 5(a) shows the simulation model. In order to enrich the information of the magnetic field distribution and improve the quality of conductivity image reconstruction, are injected independently in the experiment. The specific description is as follows:

a) The excitation electrodes contain two pairs of sliced electrodes with negligible thickness. Current can flow into the imaging body from the downside to the upside, or from left to right.

b) The excitation current is 1A, although the amplitude is beyond the human safety limit. Considering the magnetic flux density has multiple relationships with the current amplitude, before modelling and simulation by SAE, normalized the magnetic flux density, the amplitude of current will not affect the reconstruction result.

c) The sensors are located around the imaging object with equally spaced three circles, and here we put 100 sensors for each circle. The radius of the three circles of sensors' location

are 5.25 cm, 5.5 cm, and 5.75 cm. The sensors can measure the magnetic flux density surrounding the imaging body in a tangent direction.

In order to obtain the training samples of the neural network, the finite element method (FEM) is used to solve the forward problem of MDEIT. The circular imaging object with a radius of 5 cm is divided into 486 triangular elements by finite element method. Add an anomaly that occupies 20 triangle elements at random locations within the imaging body, as shown in Fig. 5 (b).

In the simulation experiment, the conductivity of the background tissue is set to 1 S/m, and the conductivity of the anomaly is 2 S/m. Surface electrodes inject the current from the left to right sides (hereinafter referred to as x-direction current), and the anomaly traversed through 486 meshed elements of the imaging body to obtain 486 sets of modelling data. Then, the imaging object is excited by electrodes on the lower and upper sides (hereinafter referred to as y-direction current), and the anomaly traversed through 486 elements of the imaging body to obtain 486 sets of data. In summary, we combine two sets of magnetic induction values corresponding to the same conductivity distribution into one column and obtain a dataset of a total of 486 different conductivity distribution and their corresponding external magnetic induction intensity distribution of the imaging body. There are a total of 600 magnetic induction values and 486 conductivity values for each set of data.

In order to evaluate the universality of the SAE algorithm to solve the MDEIT image reconstruction problem and the overall performance of the evaluation method, 400 sets of samples were randomly selected as the training data of the neural network, and the remaining 86 samples were used as the prediction data of the neural network. MDEIT using SAE neural network contains two steps: unsupervised training and fine-tuning of supervised parameters. $\boldsymbol{X} = \{\boldsymbol{x^1}, \boldsymbol{x^2}, \ldots, \boldsymbol{x^m}\}$ is the input data used to train the neural network model, where m represents the number of training samples, $\boldsymbol{x^k}$(k $= 1, 2, 3 \ldots$ m) represents the combination of two sets of independent magnetic induction components detected by 300 sensors under different electrode excitation conditions. $\mathbf{O} = \{\boldsymbol{o^1}, \boldsymbol{o^2}, \ldots, \boldsymbol{o^m}\}$ is the output data used to train the neural network model, where m represents the number of training samples, $\boldsymbol{o^k}$(k $= 1, 2, 3 \ldots$ m) represents the conductivity of 486 independent meshed elements. The structure of test data is the same as the training data.

The SAE neural network used in this study uses a 4-layer structure. As shown in Fig. 6, the number of neurons for each layer is set as {600, 559, 521, 486}. The learning rate of each layer in the training phase is 0.1, the training epochs are 3000, and the batchsize is 10. In the fine-tuning parameter phase, the learning rate is 0.1, the training epochs are 3000, and the batch-size is 10. The input vector (magnetic induction value) of the test set is used to reconstruct the conductivity distribution of the imaging body by this network. The SAE network training is completed on the computer with Intel i5-8400 CPU, 16GB RAM and NVIDIA GeForce GTX 1060 3GB.

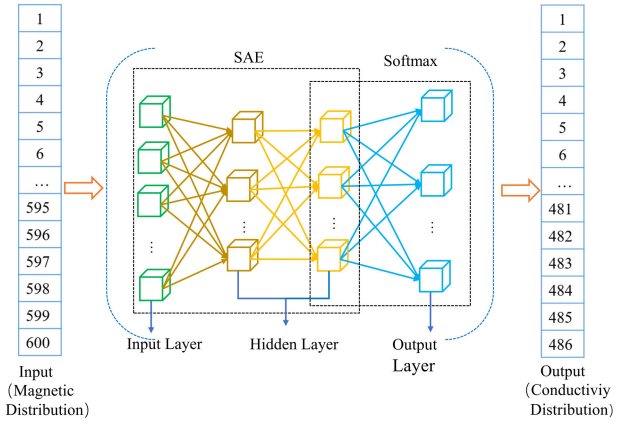

FIGURE 6. Neural network structure used in this study.

TABLE 1. Training time and prediction time of the two neural networks.

	training time/hours	prediction time/seconds
BP algorithm	1	0.2
SAE algorithm	12	0.01

The running time of the two neural networks is shown in Table 1, while the calculation time of SM algorithm is 3.5 hours. Although the training time is relatively long for training, once the network is obtained, it takes no more than 0.01s to reconstruct the conductivity image by SAE algorithm. It is fast enough for a dynamic function monitor ing.

B. NOISE EXPERIMENT

Considering there will be noises in real measurement experiment, in order to verify the anti-noise performance of the algorithm, Gaussian white noise with different magnitude levels is added to the magnetic flux density data. Then the noised magnetic flux density data are used to reconstruct the conductivity distribution by the network trained in Experiment A.

C. PHANTOM EXPERIMENT

In order to evaluate the superiority and feasibility of the proposed SAE neural network for breast cancer diagnosis by MDEIT, a phantom experiment is completed. The MDEIT experimental system is mainly composed of a space scanning platform, magnetic induction detection coil, SR7280 Lock-in Amplifier and a motor driver. The detecting coil is used to measure the magnetic induction intensity B outside the imaging body, the motor driver is used to rotate the spatial scanning platform to change the measuring position of the detecting coil and the Lock-in Amplifier is used to measure and record the magnetic induction intensity values. The experimental system is shown in Fig. 7.

A hemispherical container made of acrylic with the radius of 10 cm was used to be the phantom. Two pairs of sliced

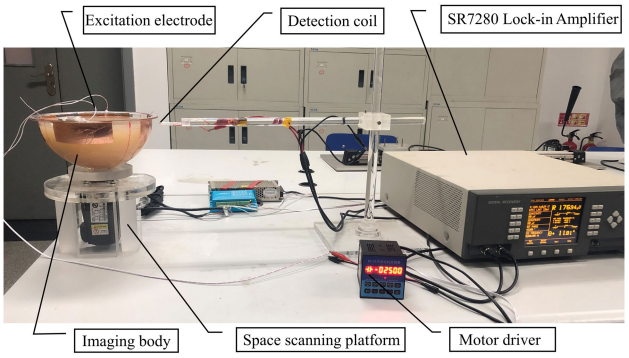

FIGURE 7. Breast phantom experiment.

FIGURE 8. The phantom used in this experiment.

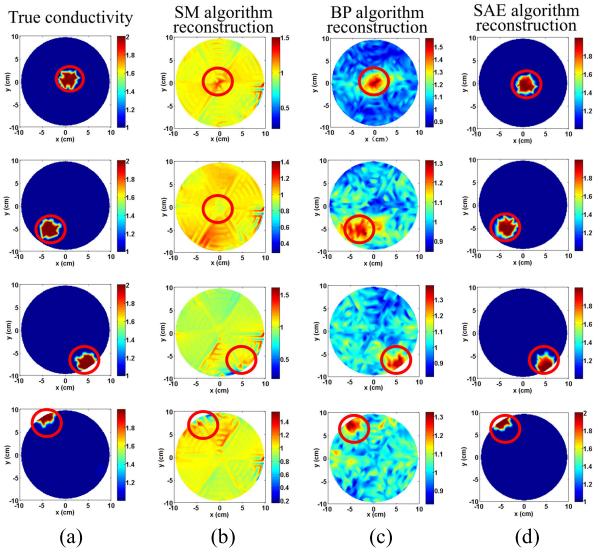

FIGURE 9. Simulation data reconstruction result. (a) represents the true conductivity, (b) represents the reconstruction results of the SM algorithm, (c) represents the reconstruction results of the BP algorithm and (d) represents the reconstruction results of the SAE algorithm.

electrodes are used as the excitation electrodes. The phantom is composed of NaCl, agar, water and an aluminum rod. Mixture of NaCl with a concentration of 9 g/L and agar of 30 g/L is mixed up in a container and heated, after the agar is gradually dissolved and fully compatible with water, it is placed in a phantom container. An aluminum rod with the radius of 2cm is inserted as the anomaly in the phantom. The phantom is shown in Fig. 8.

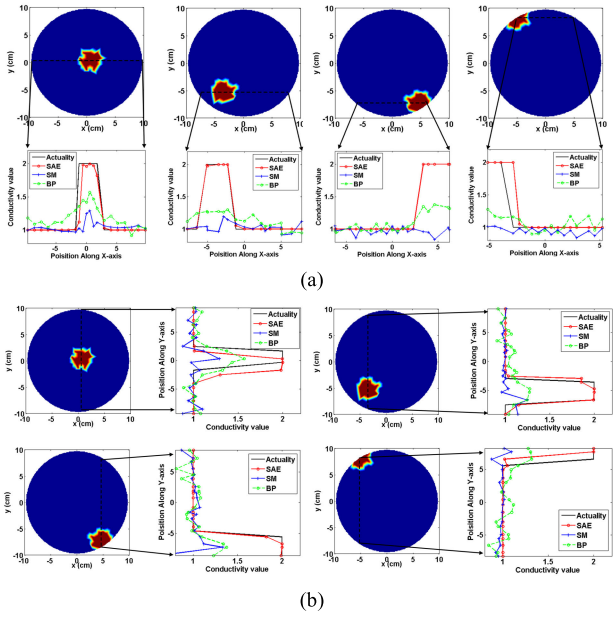

FIGURE 10. Comparison of the size and shape of anomaly conductivity in reconstruction result. Cross section plot (a) in X and cross section plot (b) in Y.

As shown in Fig. 5(b), the magnetic induction intensity sensors are located with a distance of 10.5 cm, 11cm, and 11.5 cm from the center of phantom. When the Space scanning platform rotates one circle, 100 magnetic induction values are collected. In each experiment, the scanning platform space was rotated along 3 circles and a total of 300 magnetic induction intensity values are obtained. In the case of two pairs of electrode excitation, a total of 600 magnetic induction values are obtained by MDEIT experimental system. 600 magnetic flux density values are used for conductivity reconstruction. Both BP and SAE algorithms are used in the reconstruction.

IV. RESULTS

A. SIMULATION EXPERIMENT RESULTS

In order to evaluate the advantages of SAE neural network for solving MDEIT image reconstruction problem, the reconstruction results of BP algorithm, SM algorithm and SAE algorithm are compared. Fig. 9 is a comparison of anomaly localization effects in reconstructed images of BP algorithm, SM algorithm and SAE algorithm. Each row represents a different location of the anomaly in the imaging body. In Fig. 9, Fig. 11 and Fig. 13, the red circle does not represent the outline of the anomaly but markers help to read. The results show that by the SAE algorithm, the anomalies at different positions can be accurately located in the imaging body. The reconstructed results show a poor positioning effect on the anomaly center by the SM algorithm and the BP algorithm. Only the approximate region of the anomaly can be determined by the BP algorithm. The anomaly cannot be reconstructed by the SM algorithm. Therefore, the SAE

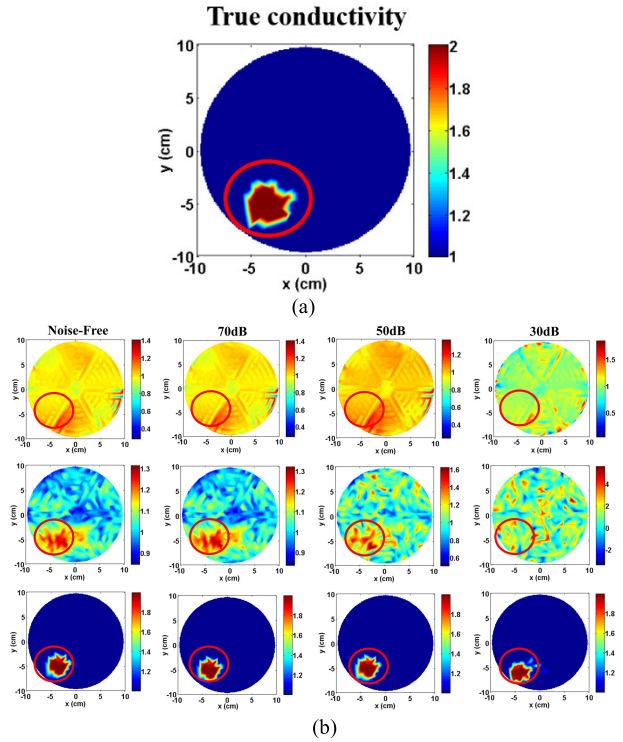

FIGURE 11. Comparison of anti-noise performance between three algorithms. (a) represents true conductivity distribution of the imaging body. Each row in (b) represents the reconstruction results of the SM algorithm, BP algorithm, and SAE algorithm respectively after adding 70dB, 50dB, and 30dB noise.

algorithm is superior to the SM algorithm and BP algorithm in the localization performance of anomalies.

Fig. 10 is a comparison of the magnitude and shape of anomaly conductivity in reconstructed images of BP algorithm, SM algorithm, and SAE algorithm. The cross-sectional view shows the distribution of the conductivity on a straight line in a two-dimensional image. It visually compares the size and shape of anomalies reconstructed by the three algorithms at different positions. The values in Table 2 are the full widths of the half maxima (FWHM) in the X and Y directions calculated from the cross-sectional view in Fig. 10, it represents a comparison of the reconstruction anomalies reconstructed by the three algorithms at different positions. As for the SM algorithm, the FWHM cannot be calculated since the reconstructed conductivity of the anomaly conductivity is close to the background conductivity value. With the BP algorithm, the conductivity values and the shape of the anomaly is different from the reality. Only the approximate position of the anomaly can be determined. However, by the SAE algorithm, the anomaly can be reconstructed correctly. The results show that the SAE algorithm is superior to the SM algorithm and the BP algorithm in the reconstruction performance of anomaly's conductivity and shape.

B. NOISE EXPERIMENT RESULTS

Fig. 11 is a comparison of the noise immunity among three algorithms. Fig. 11(a) shows the exact conductivity distribution of the image to be reconstructed, and each column of Fig. 11(b) represents different signal-to-noise ratio (SNR) levels of the measurement. The SNR is calculated as shown in (14).

TABLE 2. Comparison of reconstruction profiles corresponding to three algorithms with different anomaly locations.

		Peak	FHWM in the X direction	FHWM in the X direction
Posotion1	True value	2	4.5	3.5
	SM	1.2	1	1
	BP	1.3	3.5	4
	SAE	2	4	3.5
Posotion2	True value	2	4	4
	SM	1.2	/	/
	BP	1.3	5.5	3.5
	SAE	2	4	4.5
Posotion3	True value	3.5	3.5	3.5
	SM	/	/	/
	BP	3	3	1.5
	SAE	3.5	3.5	3.5
Posotion4	True value	2	1.5	2
	SM	1.2	/	/
	BP	1.6	3	2.5
	SAE	2	2.5	1

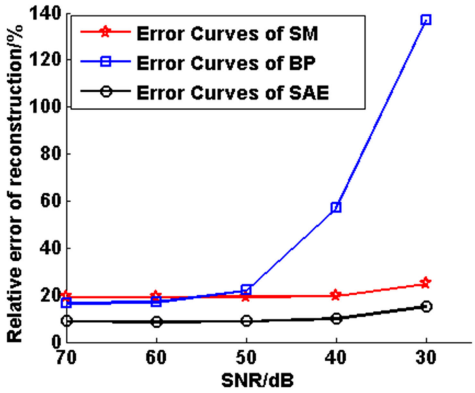

FIGURE 12. Comparison of relative errors of three algorithms with different SNR levels.

$$SNR = 10 \times log \frac{sigPower}{noisePower} \tag{14}$$

where ***sigpower*** represents the power of original signal and ***noisepower*** represents the power of noise.

Fig. 12 is a comparison of the reconstruction error curves of three algorithms at different SNR levels. The relative error of reconstruction is calculated as shows in (15).

$$R = \frac{\|\sigma_{Reconstruction} - \sigma_{Actual}\|}{\|\sigma_{Actual}\|} \times 100\% \tag{15}$$

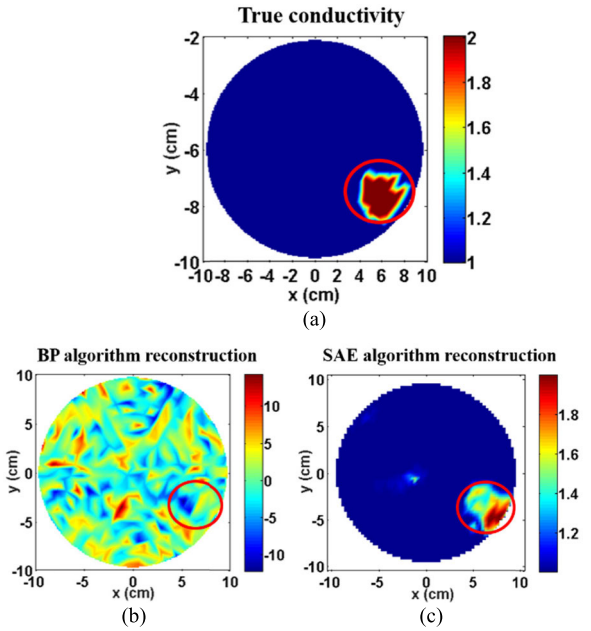

FIGURE 13. Reconstruction image and real conductivity distribution. (a) represents the true conductivity distribution, (b) represents the reconstruction conductivity distribution of the BP algorithm, and (c) represents the reconstruction conductivity distribution of the SAE algorithm.

where $\sigma_{Reconstruction}$ represents the reconstruction conductivity vector and $\sigma_{Actural}$ represents the real conductivity vector.

The experimental results show that the relative error of the SAE algorithm is still significantly lower than the other two algorithms with the increase of noise level. When the signal-to-noise ratio is 30 dB, the relative error of the SAE algorithm is 15.28%, and the location of the anomaly can still be determined. The relative errors of BP algorithm and SM algorithm are 137.19% and 24.90%, respectively. No matter by SM algorithm or BP algorithm, the location and shapes of the anomaly can't be reconstructed correctly. Therefore, the SAE algorithm is significantly more robust to noises than the other two algorithms.

C. PHANTOM EXPERIMENT RESULTS

The results of the phantom experiment are shown in Fig. 13. Fig. 13(a) is the exact conductivity distribution of the phantom used in the experiment, Fig. 13(b) is the reconstruction result of the BP algorithm, and Fig. 13(c) is the reconstruction result of the SAE algorithm. It can be seen that the position of the anomaly in Fig. 13(c) is consistent with the position of the real anomaly. In Fig. 13(b), the anomaly couldn't be reconstructed and the background of the image is not uniform. According to (15), the BP algorithm reconstruction error is 246.17%, and the SAE algorithm reconstruction error is 14.56%. It shows the promising application of the SAE algorithm for breast cancer diagnosis with MDEIT.

V. DISSCUSSION

In order to improve radiation, resolution and other issues of breast cancer detection technology, a stacked autoencoder neural network algorithm for breast cancer diagnosis with MDEIT is proposed. In order to evaluate the reconstruction performance of the algorithm, the reconstruction result of the SAE algorithm, BP algorithm and SM algorithm is compared by simulation and phantom experiment. In order to test its feasibility in real measurement environment, the anti-noise performance of the three algorithms is also analyzed with the low noise. It shows that by SAE algorithm the conductivity can be reconstructed more closely to real ones, and the location and shapes of the anomaly can be reconstructed more accurately. Both simulation and phantom experiments show that the reconstruction of SAE algorithm is superior to the other two algorithms. The proposed algorithm improves the accuracy of the reconstruction images. In addition, compared with the other two algorithms, the SAE algorithm has a shorter prediction reconstruction time. The experiments preliminarily verify the feasibility of SAE algorithm for MDEIT. It also provides a non-invasive, fast and high accuracy method for breast cancer diagnosis. However, this algorithm still has limitations that need to be improved. Though the prediction time is quite short, the training time is long. And the number of meshing elements will affect the reconstruction accuracy and reconstruction speed. A large number of samples will cause the SAE neural network training time to become long. So in the future research, the relationship between reconstruction accuracy and training time should be balanced, and more realistic experiments needs to be done.

VI. CONCLUSION

In this paper, a new algorithm based on stacked autoencoder neural network is proposed for breast cancer diagnosis by MDEIT. Both simulation and phantom experiments show that by the SAE algorithm, the internal conductivity distribution of the imaging body can be reconstructed correctly using the magnetic flux density surrounding the body. The contour of the anomaly is reconstructed clearly and the location of the anomaly is reconstructed accurately. The proposed SAE algorithm is of great significance to the development of MDEIT and lays the foundation of electrical impedance tomography to clinical application of breast cancer diagnosis. It can also provide a support for the other applications of MDEIT technology.

REFERENCES

[1] G. Mustacchi and M. De Laurentiis, "The role of taxanes in triple-negative breast cancer: Literature review," *Drug Des. Develop. Therapy*, vol. 9, pp. 4303–4318, Sep. 2015.

[2] R. Vijayarajeswari, P. Parthasarathy, S. Vivekanandan, and A. A. Basha, "Classification of mammogram for early detection of breast cancer using SVM classifier and Hough transform," *Measurement*, vol. 146, pp. 800–805, Nov. 2019.

[3] G. L. Shi, F. Han, C. W. Liang, L. Wang, and K. Y. Li, "A novel method of thermal tomography tumor diagnosis and its clinical practice," *Appl. Thermal Eng.*, vol. 73, no. 1, pp. 408–415, Dec. 2014.

[4] D. Cai, T. Lin, K. Jiang, and Z. Sun, "Diagnostic value of MRI combined with ultrasound for lymph node metastasis in breast cancer: Protocol for a meta-analysis," *Medicine*, to be published, doi: 10.1097/MD.0000000000016528.

[5] R. H. Ireland, J. C. Tozer, A. T. Barker, and D. C. Barber, "Towards magnetic detection electrical impedance tomography: Data acquisition and image reconstruction of current density in phantoms and *in vivo*," *Physiol. Meas.*, vol. 25, no. 3, pp. 775–796, Jun. 2004.
[6] R. H. Ireland and D. C. Barber, "Constrained image reconstruction for magnetic detection electrical impedance tomography," *Int. J. Imag. Syst., Technol.*, vol. 17, no. 6, pp. 379–382, Dec. 2007.
[7] Y. Wang, S. Ren, and F. Dong, "Focusing sensor design for open electrical impedance tomography based on shape conformal transformation," in *Sensors*, Bath, U.K., 2018, pp. 2–22.
[8] L. Hao, G. Li, and L. Lin, "Optimization of measurement arrangements for magnetic detection electrical impedance tomography," *IEEE Trans. Biomed. Eng.*, vol. 61, no. 2, pp. 444–452, Feb. 2014.
[9] D. Zhu, A. McEwan, and C. Eiber, "Microelectrode array electrical impedance tomography for fast functional imaging in the thalamus," *NeuroImage*, vol. 198, pp. 44–52, Sep. 2019.
[10] G. Li, L. Hao, R. Chen, and L. Lin, "A new electrode mode for magnetic detection electrical impedance tomography: Computer simulation study," *IEEE Trans. Magn.*, vol. 48, no. 10, pp. 2543–2550, Oct. 2012.
[11] R. J. Sadleir, F. Fu, C. Falgas, S. Holland, M. Boggess, S. C. Grant, and E. J. Woo, "Direct detection of neural activity *in vitro* using magnetic resonance electrical impedance tomography (MREIT)," *NeuroImage*, vol. 161, pp. 104–119, Nov. 2017.
[12] K. Liu, Y. Fan, Z. Songyang, Z. Liwei, H. Jiayuan, W. Xiaoyu, and I. Ullah, "Research on grounding grids imaging reconstruction based on magnetic detection electrical impedance tomography," *IEEE Trans. Mag.*, vol. 54, no. 3, Mar. 2018, Art. no. 4600204.
[13] L. L. Hao, G. Li, and L. S. Xu, "Magnetic detection electrical impedance tomography with total variation regularization," *Bio-Med. Mater. Eng.*, vol. 24, no. 6, pp. 2857–2864, 2014.
[14] M. K. Choi, B. Harrach, and J. K. Seo, "Regularizing a linearized EIT reconstruction method using a sensitivity-based factorization method," *Inverse Problems Sci. Eng.*, vol. 22, no. 7, pp. 1029–1044, 2014.
[15] A. Javaherian, M. Soleimani, K. Moeller, A. Movafeghi, and R. Faghihi, "An accelerated version of alternating direction method of multipliers for TV minimization in EIT," *Appl. Math. Model.*, vol. 40, nos. 21–22, pp. 8985–9000, May 2016.
[16] G. González, V. Kolehmainen, and A. Seppänen, "Isotropic and anisotropic total variation regularization in electrical impedance tomography," *Comput. Math. Appl.*, vol. 74, no. 3, pp. 564–576, Aug. 2017.
[17] J. N. Tehrani, A. McEwan, C. Jin, and A. van Schaik, "L1 regularization method in electrical impedance tomography by using the L1-curve (Pareto frontier curve)," *Appl. Math. Model.*, vol. 36, no. 3, pp. 1095–1105, Mar. 2012.
[18] L. Zhang, H.-K. Lam, Y. Sun, and H. Liang, "Fault detection for fuzzy semi-Markov jump systems based on interval type-2 fuzzy approach," *IEEE Trans. Fuzzy Syst.*, to be published, doi: 10.1109/TFUZZ.2019.2936333.
[19] P. Du, H. Liang, S. Zhao, and C. K. Ahn, "Neural-based decentralized adaptive finite-time control for nonlinear large-scale systems with time-varying output constraints," *IEEE Trans. Syst.*, to be published, doi: 10.1109/TSMC.2019.2918351.
[20] L. Zhang, H. Liang, Y. Sun, and C. K. Ahn, "Adaptive event-triggered fault detection scheme for semi-Markovian jump systems with output quantization," *IEEE Trans. Syst.*, doi: 10.1109/TSMC.2019.2912846.
[21] B. L. Liu and A. B. Djamel, "Effective image super resolution via hierarchical convolutional neural network," *Neurocomputing*, vol. 374, pp. 109–116, Jan. 2020.
[22] M. S. Hossain and G. Muhammad, "Emotion recognition using secure edge and cloud computing," *Inf. Sci.*, vol. 504, pp. 589–601, Dec. 2019.
[23] J. Zheng and L. Peng, "An autoencoder-based image reconstruction for electrical capacitance tomography," *IEEE Sensors J.*, vol. 18, no. 13, pp. 5464–5474, Jul. 2018.
[24] H. Wang, N. Wu, Y. Cai, L. Ren, Z. Zhao, G. Han, and J. Wang, "Optimization of reconstruction accuracy of anomaly position based on stacked auto-encoder neural networks," *IEEE Access*, vol. 7, pp. 116578–116584, Aug. 2019.
[25] K. H. Jin, M. T. McCann, E. Froustey, and M. Unser, "Deep convolutional neural network for inverse problems in imaging," *IEEE Trans. Image Process.*, vol. 26, no. 9, pp. 4509–4522, Sep. 2017.
[26] D. Boublil, M. Elad, J. Shtok, and M. Zibulevsky, "Spatially-adaptive reconstruction in computed tomography using neural networks," *IEEE Trans. Med. Imag.*, vol. 34, no. 7, pp. 1474–1485, Jul. 2015.
[27] N. Gao, S. A. Zhu, and B. He, "Estimation of electrical conductivity distribution within the human head from magnetic flux density measurement," *Phys. Med. Biol.*, vol. 50, no. 11, pp. 2675–2687, Jun. 2005.
[28] T. Menden, J. Orschulik, S. Dambrun, J. Matuszczyk, S. A. Santos, S. Leonhardt, and M. Walter, "Reconstruction algorithm for frequency-differential EIT using absolute values," *Physiol. Meas.*, vol. 40, no. 3, 2019, Art. no. 034008, doi: 10.1088/1361-6579/ab0b55.
[29] O. Birgul, B. M. Eyuboglu, and Y. Z. Ider, "Experimental results for 2D magnetic resonance electrical impedance tomography (MR-EIT) using magnetic flux density in one direction," *Phys. Med. Biol.*, vol. 48, no. 21, pp. 3485–3504, Nov. 2003.
[30] M. Bonazzoli, V. Dolean, I. G. Graham, E. A. Spence, and R. H. Tournier, "Domain decomposition preconditioning for the high-frequency time-harmonic Maxwell equations with absorption," *Math. Comput.*, vol. 88, pp. 2559–2604, May 2019.
[31] K. M. Bakhshayesh, "Comparative study of application of different supervised learning methods in forecasting future states of NPPs operating parameters," *Ann. Nucl. Energy*, vol. 132, pp. 87–99, Oct. 2019.
[32] G. Lu, H. Zhang, and X. G. Tang, "A novel method for intelligent single fault detection of bearings using SAE and improved D-S evidence theory," *Entropy*, vol. 21, no. 7, pp. 92410–92418, Jul. 2019.
[33] R. Jiao, X. Huang, X. Ma, L. Han, and W. Tian, "A model combining stacked auto encoder and back propagation algorithm for short-term wind power forecasting," *IEEE Access*, vol. 6, pp. 17851–17858, Mar. 2018.
[34] Y. He, C. Li, T. Wang, T. Shi, L. Tao, and W. Yuan, "Incipient fault diagnosis method for IGBT drive circuit based on improved SAE," *IEEE Access*, vol. 7, pp. 92410–92418, Jun. 2019.
[35] Z. Li, J. Li, Y. Wang, and K. Wang, "A deep learning approach for anomaly detection based on SAE and LSTM in mechanical equipment," *Int. J. Adv. Manuf. Technol.*, vol. 103, nos. 1–4, pp. 499–510, Jul. 2019.
[36] H. Yin, X. Jiao, Y. Chai, and B. Fang, "Scene classification based on single-layer SAE and SVM," *Expert Syst. Appl.*, vol. 42, no. 7, pp. 3368–3380, May 2015.
[37] H. I. Suk, S.-W. Lee, D. Shen, and The Alzheimer's Disease Neuroimaging Initiative, "Latent feature representation with stacked auto-encoder for AD/MCI diagnosis," *Brain Struct. Function*, vol. 220, no. 2, pp. 841–859, Mar. 2015.

RUIJUAN CHEN was born in 1984. She received the bachelor's degree from Hebei University, in 2006, the master's degree from the Hebei University of Technology, in 2009, and the Ph.D. degree from Tianjin University, in 2012. From 2012 to 2014, she was involved in research at the National Micro Imaging Center, University of California, San Diego, CA, USA. She is currently a Master Instructor with the School of Life's Sciences, Tiangong University. Her main research interests include biomedical imaging, biomedical image processing, and biomedical information detection.

WEIWEI WU was born in 1995. She received the bachelor's degree in electronic information science and technology from Xinzhou Teachers University. She is currently pursuing the master's degree in electronics and communication engineering with the School of Electronics and Information Engineering, Tiangong University. Her main research directions include biomedical imaging and biomedical image processing.

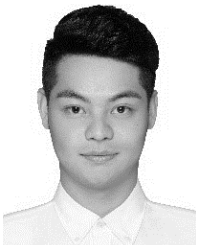

HAOFENG QI was born in 1995. He received the bachelor's degree in biomedical engineering from the School of Electronics and Information Engineering, Tiangong University, in 2016, and the master's degree in biomedical engineering from the School of Life Sciences, Tiangong University, in 2019. His main research directions include biomedical imaging and biomedical image processing.

JINHAI WANG was born in 1966. He received the bachelor's degree from Xi'an Jiaotong University, the master's degree from Tianjin Textile Institute, and the Ph.D. degree from Tianjin University. He is currently a Professor and also a Master Instructor with Tiangong University. He is the founder of the Tianjin Key Laboratory of Optoelectronic Detection Technology and Systems. He has published more than 100 articles. His main research directions include embedded system development and application, information detection and intelligent processing, medical electronic diagnosis and treatment technology and instruments, and modern sensing technology and systems.

HUIQUAN WANG was born in 1985. He received the bachelor's and Ph.D. degrees in biomedical engineering with the School of Precision Instruments and Optoelectronics Engineering, Tianjin University, and the bachelor's degree of international finance from Nankai University. He holds the postdoctoral position in instrument science and technology at Tianjin University. From 2011 to 2013, he was a Public Visiting Scholar at Johns Hopkins University. He is currently the Director of the Department of Biomedical Engineering and the Master Instructor of Tiangong University. His main research directions include wearable medical testing equipment and intervention methods, near-infrared spectroscopy and big data mining algorithms, and multimodal imaging technology.